Studies of columns of beads under external vibrations

S. Luding,[1] E. Clément,[2] A. Blumen,[1] J. Rajchenbach,[2] and J. Duran[2]
[1]*Theoretische Polymerphysik, Universität Freiburg, Rheinstrasse 12, D-79104 Freiburg, Germany*
[2]*Laboratoire d'Acoustique et d'Optique de la Matière Condensée, Université Pierre et Marie Curie, 4, place Jussieu, 75005 Paris, France*
(Received 15 June 1993; revised manuscript received 18 October 1993)

As a toy model for dissipative granular materials, we investigate a one-dimensional column of beads undergoing external vibrations. The analysis is both experimental and numerical. We display the crossover from a condensed to a fluidized state of the column; the parameters are the agitation, the number of beads, and the momentum restitution coefficient. We find clustered states for high dissipation and/or a large number of beads. Our experimental findings support the appearance of a fluidized regime at low dissipation and of a Feigenbaum-type bifurcation scenario at high dissipation.

PACS number(s): 46.10.+z, 05.60.+w, 05.40.+j

I. INTRODUCTION AND BACKGROUND

Recent years have seen a resurgence of interest in the behavior of granular media (see, for instance, Ref. [1]). Noncohesive granular materials are characterized by being assemblies of solid, nonuniform particles, which interact via contact forces and are kept together by the action of gravity. If the contact between the particles is broken, their interaction ceases.

For example, a dry sandpile belongs to this class of materials. Such systems exhibit surprising properties, for instance, a limiting slope for the free surface, spontaneous heaping under vibration, non-Newtonian shearing, etc. These are examples of properties which lie between those of solids and those of liquids, and they establish the granulates as being a quite specific and intriguing class of materials. The *a priori* assessment of macroscopic parameters from the consideration of local-contact, dissipative interactions is a difficult problem, because of the high level of disorder involved. It is evidently extremely difficult to probe the dynamics of granulated particles on scales comparable to their dimensions. Nonetheless recent years have seen big advances in the possibilities to monitor model systems on short scales [2,3]. Overall, such systems are by far more accessible than powders or sand, and they provide a probate means to investigate the basic, complex behavior of real granulates. Also the measurement of fundamental quantities such as the local densities and the energy transfer between grains requires much diligence. Furthermore, numerical simulations [4–12] are a very adequate tool to study complex dynamics, a tool which complements nicely the experimental findings [2,3,12,13], and the more analytical approaches [14,15].

In this paper we are interested in the behavior of granular materials which undergo external vertical vibrations. Note that this is a probate means of particle transport of wide industrial use. Furthermore, experiments on sandpiles in three dimensions (3D) have shown many interesting aspects, such as spontaneous heaping formation [16,17]. These findings are corroborated by the behavior of 2D model media, where experiments and simulations show spontaneous fluxes of matter, heaping, fluidization, and block motion [2,4–7]. Also these phenomena depend on the local mechanical interactions such as the friction coefficients of the beads. Here we focus on the problem of fluidization, as different from problems characterizing convection. A convenient way to achieve this separation is to take a basically one-dimensional model, i.e., a column consisting of N beads, which undergo dissipative collisions. The aim of such a model is both to have a transparent theoretical situation, as well as an experimentally manageable arrangement. The one-dimensional problem of interest here bridges also between simpler models such as the one-bead problem in 1D [18–20] and the many-bead problem in dimensions larger than one [3,5–7,21–24]. In our 1D system we neglect rotational motions and have the advantage that the beads keep their order during the whole process. Even without effects like convection or heaping our system shows the fluidization of granular materials under vibration. Thus we expect from our approach insights into the complicated and analytically involved problem of real granulates.

The one-bead problem was studied extensively both from the experimental [19] and also from the analytical and simulational [18–20] points of view. In the one-bead problem many physical effects such as period doubling can be found. On the other hand, simulating granular media realistically (for $D > 1$) is an arduous task; under the many methods which have been used we recall the time-driven Monte Carlo [24] and molecular-dynamics simulations [21–23,25–27] as well as event-driven algorithms [7–10,12,28]. We mention first the work by Cundall and Strack [5], who follow the motion of the particles via a molecular-dynamics scheme. Moreau and Jean [6,29] solve the problem numerically, by using a time-discretization procedure to follow the systems' dynamics via a set of nonsmooth equations. Other procedures are event driven, such as the one described recently by Lubachevsky [7] (who presented an algorithm to create a random packing of billiard balls) and the method of Bernu and Mazighi, who calculated the behavior of a horizontal array of beads colliding with a wall [8].

McNamura and Young simulated the same model [9] and focused on the "cooling" of one-dimensional granular media [10]. It is important to notice that in spite of the wealth of recently obtained computer results on complex systems, benchmark experiments which are connected to straightforward simulation algorithms are still lacking.

In an earlier study [12] we presented some results of simulations and experiments on columns of beads, where we found that the columns fluidized, condensed, and clustered. Reference [12] focused on condensation and clusterization; additional work is in progress [30]. In the present work we give the conditions for observing the different regimes and display scaling for fluidized systems. We corroborate these findings with experimental results, which we also present here.

In Sec. II we focus on the experimental setup. The numerical procedure is discussed mainly in Sec. III and in Appendix A. The outcome of our numerical work is presented and discussed in Sec. IV. We devote Sec. V to the comparison of the experimental findings with the numerical results, especially in what fluidization aspects are concerned.

II. THE MODEL SYSTEM

In both experiments and numerical simulations we use a system of N beads. In the experiment the beads have a well-defined diameter of $d=2.99$ mm and are enclosed in a cell, which is a vertical groove of both width and depth $d=3$ mm, cut in a rectangular block of brass of height 85 mm; a glass window in the front allows the visualization. The horizontal bottom of the groove consists of a glass plate. The plate is driven by a sinusoidal motion with amplitude A_0 and frequency f (radial frequency $\omega=2\pi f$); hence its position at time t is

$$z_0(t)=A_0\sin(\omega t)\ . \tag{1}$$

A schematic drawing is given in Fig. 1.

A charge-coupled device (CCD) camera hooked to an image processing device allows us to monitor the experiments. Furthermore, we also record the sound created by the collisions of the beads, through a microphone which is connected to a memory oscilloscope. Because of the geometry, the beads are aligned so that each bead interacts only with its upper and lower neighbors or, for the lowest bead, with the vibrating bottom plate. In the simulations we neglect the contacts the beads have with the walls of the groove and assume that the kinetic energy is lost only due to the inelasticity of the collisions. The fundamental parameter which describes this dissipation is the restitution coefficient ϵ of the momentum for a collision between beads. In the simulations we account for collisions between two individual beads (binary collisions) as well as for collisions which involve several beads in contact (clusters). The general numerical approach is introduced in the next section and the details of the procedure are described in Appendix A.

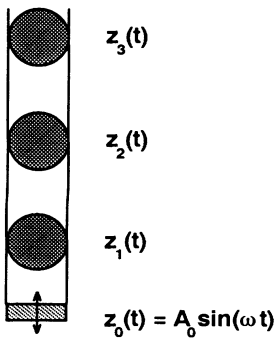

FIG. 1. Model system with a vibrating bottom plate; here three beads are shown.

We remark that the restitution coefficient ϵ is material dependent; also collisions of the lowest bead with the bottom plate may have a different restitution coefficient, which we denote by ϵ_p. In order to examine the two limiting cases of high and of low dissipation, we experimented with beads made of aluminum and stainless steel, respectively. We measured ϵ in a rough manner by the method of rebound and obtained $\epsilon=0.60\pm0.05$ for aluminum on aluminum and $\epsilon=0.90\pm0.05$ for stainless steel on stainless steel.

III. NUMERICAL PROCEDURE

The simulation consists in monitoring a sequence of events (i.e., collisions) between which Newton's equations of motion for each object are solved exactly. Here an object is an individual bead, the vibrating bottom plate, or a cluster of beads (i.e., a collection of beads in physical contact and moving with the same velocity). For an object, an event is defined either by a sudden change in momentum (collision) or by the takeoff from the bottom plate (when the upward acceleration gets larger than the gravity, denoted by g). In the following, the N beads are numbered from the bottom starting with $i=1$; for the bottom plate we set $i=0$. Between events each object i follows its own trajectory; this is so because we assume dissipation to occur only on collision. Due to the one-dimensional nature of the model, the order of beads never changes and we may even dispense with accounting for the diameter d of the beads. This fact allows us to simplify the notation in the simulations; we use diameter-independent coordinates $z_i(t)$, which are connected to the usual coordinates $z_i^*(t)$ through $z_i(t)=z_i^*(t)-(i-1)d-\frac{1}{2}d$.

With Δt denoting the time elapsed since the time t_0, the position of particle i at time $t_0+\Delta t$ is

$$z_i(\Delta t)=z_{i,0}+v_{i,0}\Delta t-\tfrac{1}{2}g(\Delta t)^2\ , \tag{2}$$

where $z_{i,0}$ and $v_{i,0}$ are the coordinates and velocities of particle i at time t_0.

We now compute the time after which the next event (i.e., between object i and $i-1$) happens. Events occur whenever $z_i(\Delta t)=z_{i-1}(\Delta t)$; this leads to a time step:

$$\Delta t_i=-\frac{z_{i,0}-z_{i-1,0}}{v_{i,0}-v_{i-1,0}}\ . \tag{3}$$

Formally these event times Δt_i are stored in an event time array T. If $\Delta t_i<0$ the objects move away from each other. If $\Delta t_i=0$ the particles are in contact, a case which

will be discussed later in this section. Of interest are now the positive Δt_i, of which the smallest, $\Delta t_{\min}$, determines the occurrence of the next event. Once the next event is identified we compute the positions and velocities of all objects at this time $t_0+\Delta t_{\min}$, carry out the transformation corresponding to the event, and update the event time array; then we look for the following event.

As already mentioned, the simulations take care of the energy loss on collisions through the dissipation coefficients ϵ and ϵ_p; furthermore, this is the only way we account for energy losses. In the reference frame of the center of mass of a colliding pair, the incoming velocities are $+V$ and $-V$ and the outgoing velocities are $-\epsilon V$ and $+\epsilon V$. Using a matrix formalism [8–10,12], this prescription reads

$$\begin{pmatrix} u_{i-1} \\ u_i \end{pmatrix} = C_{i-1,i} \begin{pmatrix} v_{i-1} \\ v_i \end{pmatrix} = \begin{pmatrix} \frac{1-\epsilon}{2} & \frac{1+\epsilon}{2} \\ \frac{1+\epsilon}{2} & \frac{1-\epsilon}{2} \end{pmatrix} \begin{pmatrix} v_{i-1} \\ v_i \end{pmatrix} \quad (i=2,\ldots,N), \tag{4}$$

where v_i and u_i are the velocities of bead i, just before and after the collision, in the system's frame of reference. A similar form holds also for collisions with the moving bottom plate, which will be assumed to have infinite mass. In the reference frame of the plate bead 1 has just before the collision a velocity V and after the collision the velocity $-\epsilon_p V$. In the collision matrix scheme [8] it follows that

$$\begin{pmatrix} u_0 \\ u_1 \end{pmatrix} = C_{0,1} \begin{pmatrix} v_0 \\ v_1 \end{pmatrix} = \begin{pmatrix} 1 & 0 \\ 1+\epsilon_p & -\epsilon_p \end{pmatrix} \begin{pmatrix} v_0 \\ v_1 \end{pmatrix} \tag{5}$$

in the system's frame of reference.

We proceed by noting that in some regions of the parameter space (i.e., for high dissipation, that corresponds to low ϵ, or at times when the acceleration of the bottom plate is low) the time intervals between the events may get to be very short. If such series of small time intervals occur, then the computing time (which is proportional to the number of events) may get very large. In the following we show how to deal with this problem. For this we focus on simulations with low restitution coefficients. We start with a column of $N=10$ beads. As initial conditions we take an equidistant separation between beads (here 1 mm) and a random distribution of velocities (here -1 m/s $< v_i < 1$ m/s). For the restitution coefficients we take $\epsilon=0.6$ and $\epsilon_p=1$ (which is typical for aluminum beads and a bottom plate made of glass). Then we record as a function of time the trajectories of the beads, as well as the times $\Delta t^{(m,m-1)}$ between events (the events are numbered sequentially, $m=1,2,3,\ldots$). This situation is depicted in Fig. 2. In the upper part of the picture we plot the actual positions of the beads (the diameter of the beads is—as noted before—disregarded); the dotted line gives the position of the bottom plate. Remember that the order of particles does not change; this means that the trajectory of one particle does not cross the trajectory of another, but that their slopes change abruptly at the time of a collision. The time intervals $\Delta t^{(m,m-1)}$ between

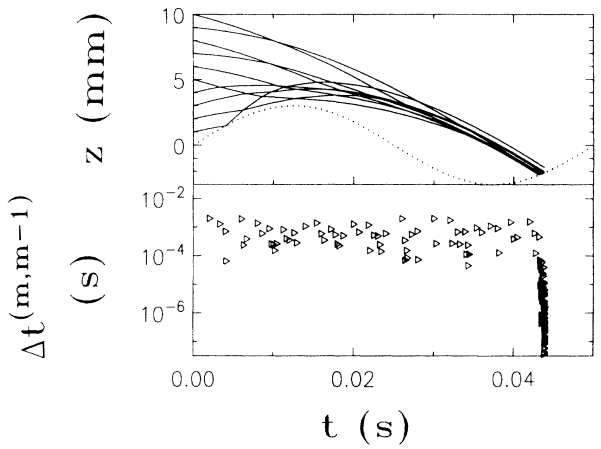

FIG. 2. Motion of ten beads where the restitution coefficients are $\epsilon=0.6$ and $\epsilon_p=1$ (see text for details). The upper part displays the trajectories and the dotted line indicates the bottom plate; the lower part gives the time intervals $\Delta t^{(m,m-1)}$ between events.

events are given on a logarithmic scale in the lower part of the picture and are represented by triangles. One should remark that a sudden decrease in the time intervals between events is noticeable in Fig. 2 for $t \cong 0.044$ s. Moreover, at this moment both the distances between the beads involved in the events, $\Delta z_i = z_i - z_{i-1}$, as well as their relative velocities, $\Delta v_i = v_{i-1} - v_i$, get to be very small ($\Delta v_i > 0$ before and $\Delta v_i < 0$ after a collision). Evidently at such moments the event-driven algorithm runs into a situation which is computationally very time-consuming. It is furthermore also not of physical interest to follow the procedure on such short time and length scales, because when the times between events become very small, our macroscopic description of the dissipation via ϵ and ϵ_p becomes questionable.

A means to avoid such problems is to introduce a cutoff velocity v_c. The idea is to merge objects which after the event have a relative velocity $|\Delta u_i| < v_c$ into a cluster, while at the same time one conserves the momentum of the center of mass of the newly created cluster. The description therefore leads from independent objects before the event to a new object, a cluster, in which the objects have zero relative distance between them and have (of course) the same velocity, after the event. We are justified in proceeding in this way also by the results of Refs. [8–10], in which it was found that in the case of high dissipation clusterization occurs; this means that there is a total loss of relative momentum.

We choose v_c to be orders of magnitude smaller than the typical velocity $A_0\omega$ of the system (typical values are $A_0=10^{-3}$ m and $f=20$ Hz, which lead to $A_0\omega=0.125$ m/s; we usually take v_c around 10^{-7} m/s, so that $v_c \ll A_0\omega$). By varying v_c we ascertained that the specific choice of v_c does not change the results of the simulation, as long as v_c and $A_0\omega$ differ by orders of magnitude.

Our shift of point of view, consisting in replacing individual beads by clusters, must now be supplemented by a

procedure which determines how collisions of such clusters (with the bottom plate, with another individual bead, or with another cluster) have to be handled. In Appendix A we give a detailed description of the algorithm involved. The basic idea is to take a relative velocity scheme, and assume that the next event in the cascade is the one for which the relative velocity $\Delta v_i = v_{i-1} - v_i$ is maximal. This is based on the fact that, as described above, one runs into problems when one uses time differences to establish the order in which the collisions happen. For beads in contact (or almost in contact with each other) a collision with an external bead leads to a cascade of events involving other inner beads. In the algorithm described in Appendix A one takes as next event the one for which the relative velocity is maximal.

IV. RESULTS OF SIMULATIONS

We turn now to a discussion of the results of our simulations. The parameters involved are the number of beads N, the restitution coefficients ϵ_p and ϵ, as well as the amplitude A_0 and the angular frequency $\omega = 2\pi f$. Some numerically established data are experimentally accessible; these are then compared in Sec. V with the measurements.

A. The transition from a fluidized to a condensed regime

For restitution coefficients close to one and at high accelerations of the bottom plate the individual motion of the beads looks erratic. This is what we call *fluidization.* If the input energy is decreased, the motion becomes more and more regular and the column of beads eventually gets locked on the excitation period. This is what we call *condensation.* In Fig. 3 we show three typical behaviors of the column depending on the input energy of the system. The parameters used are $N = 10$, $f = 20$ Hz, $\epsilon_p = 1$, and $\epsilon = 0.92$. The amplitude A_0 varies from 4.97 mm in Fig. 3(a) to 1.24 mm in Fig. 3(b) and 0.932 mm in Fig. 3(c). An important dimensionless parameter is α, the maximal acceleration of the bottom plate divided by the acceleration of gravity g:

$$\alpha = \frac{A_0 \omega^2}{g} . \tag{6}$$

In Figs. 3(a), 3(b), and 3(c), α is 8.0, 2.0, and 1.5, respectively. The trajectories of the particles show the progressive condensation of the column. To illustrate this change of behavior we use a gray code: light gray indicates high velocities and dark gray low velocities. It is evident from Fig. 3 that for lower values of the acceleration the motion is collective; at higher acceleration values we find that the role of the fluctuations increases. In the insets of Fig. 3 we show the frequency spectra obtained through a fast Fourier transform (FFT) algorithm for the motion of the center of mass (c.m.). In the FFT algorithm the position of the diameter-dependent height of c.m. ($h_{\text{c.m.}}$) was evaluated 25 times per period during a total of some 328 periods, within which 2^{13} data points were obtained. At higher energies still, the motion of the c.m. displays a continuous spectrum [Fig. 3(a)]. When the input energy decreases, the motion of the center of mass begins to show the harmonics and the subharmonics of the excitation frequency [Fig. 3(b)]. If the energy decreases still [Fig. 3(c)], a Feigenbaum scenario is observed, a bifurcation cascade which displays period doubling.

The passage from a fluidized state [Fig. 3(a)—note the quasiballistic trajectories for the momentum waves] to a state involving collective motions of the column [Figs. 3(b) and 3(c)] is gradual. To monitor this behavior, we look at the mean dilatation of the column $\langle z_N - z_1 \rangle$ where z_1 and z_N are the height of the first and the Nth particle. We recall that the z_i coordinates are indepen-

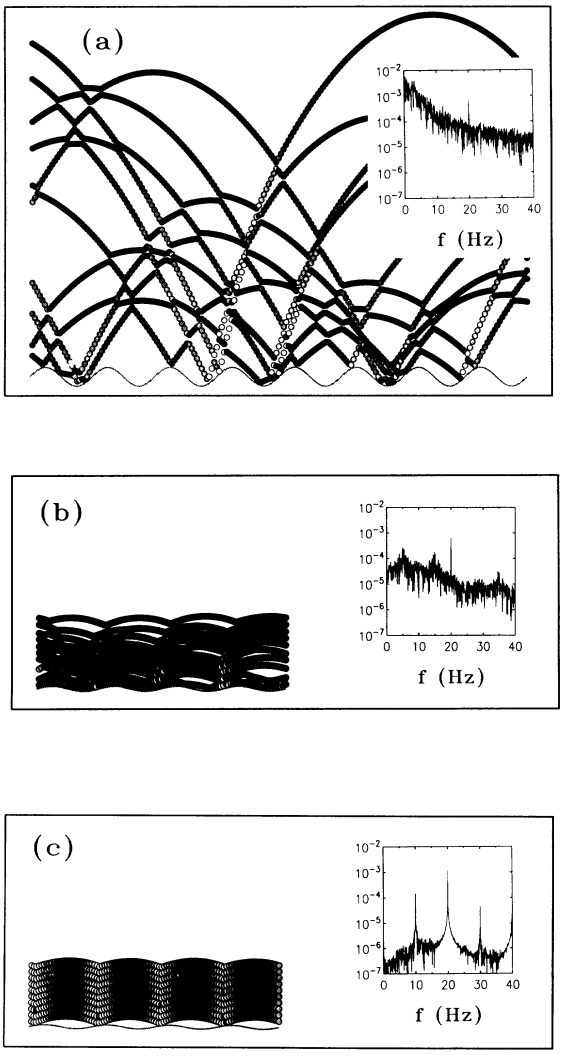

FIG. 3. (a) Motion of ten beads for $f = 20$ Hz, $\alpha = 8.0$, $\epsilon = 0.92$, and $\epsilon_p = 1$. The inset displays the frequency spectrum for the motion of the center of mass (c.m.). (b) Motion of ten beads for $f = 20$ Hz, $\alpha = 2.0$, $\epsilon = 0.92$, and $\epsilon_p = 1$. The inset displays the frequency spectrum for the motion of the center of mass. (c) Motion of ten beads for $f = 20$ Hz, $\alpha = 1.5$, $\epsilon = 0.92$, and $\epsilon_p = 1$. The inset displays the frequency spectrum for the motion of the center of mass.

dent of the bead diameters, see Sec. III. The mean dilatation is a good indicator of clusterization. In Fig. 4 we depict the dilatation using the dimensionless quantity λ:

$$\lambda = \frac{\langle z_N - z_1 \rangle}{A_0 \alpha} . \tag{7}$$

We display λ as a function of α for $N=8$, 10, and 12, while keeping $\epsilon=0.92$ constant. The frequencies used are $=10$, 20, 40, 80, 100, 200, 400, and 800 Hz and we vary the amplitude A_0. Note that for a given N, all the curves collapse on the same master curve. For high-energy input (corresponding to large α values) λ converges to a constant. Since in this limit we have $\langle z_1 \rangle \ll \langle z_N \rangle$, for fixed N the mean dilatation is proportional to the potential energy; the scaling behavior, Eq. (7), thus indicates that $\langle z_N - z_1 \rangle$ and hence also the potential energy are proportional to $A_0\alpha$. Therefore in the fluidized regime the potential energy scales with $A_0^2\omega^2$. In other words, in the fluidized limit a proper scaling parameter is the squared velocity $(A_0\omega)^2$ and not the acceleration α. If α gets lower (say for $\alpha < 10$) the column behaves in a complex fashion and resonances may show up. But α is not the only control parameter for the occurrence of condensation; for different N we find different behavior for the same α values. Thus columns with larger N show less dilatation. This is due to the fact that the number of dissipative contacts increases with N; a system with larger N displays a higher dissipation. Note that for a dissipative block (or a completely inelastic particle) on a vibrating plate, the pertinent control parameter is the relative acceleration α [18–20]. As a result one has a very complex transition between the *clustered* regime, a transition which depends on N, on ϵ, and also on α.

In the fluidized regime, the erratic motion of particles and the large dilatation of the column may suggest some analogy with the behavior of a dense gas column when connected to a heat bath, and in general to thermodynamic concepts. Mazighi, Bernu, and Deylon [28] recently found an analytic description for a one-dimensional array of beads where the bottom plate follows a triangular instead of a sinusoidal function. There they find, using the dissipative Boltzmann equation, in the limit of low dissipation, a density profile which is nearly exponential. We remark that the function of the bottom plate is analogous to a heat bath in providing (and sometimes taking away) energy from the system. Furthermore, we like to point out that other thermodynamic and/or hydrodynamic ideas have been advanced to describe a granular assembly [31–33]. Thus 1D columns of beads seem to be good candidates to test the relevance of such an approach. But one has to pay attention to the fact that even in such "one-dimensional" systems experimentally additional effects (such as rotations) may appear and that important aspects of realistic three-dimensional systems are neglected.

Here we are interested in the qualitative features of the density and of the kinetic energy distributions. In Fig. 5(a) we present the density of the beads as a function of the height. The density is evaluated for $N=10$, $\epsilon=0.92$, and $f=20$ Hz. Here we use the diameter-dependent

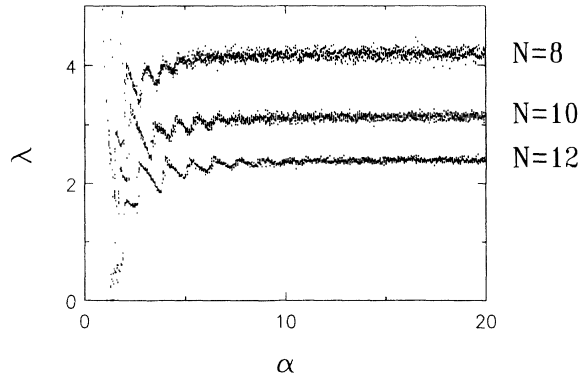

FIG. 4. Mean dilatation λ plotted versus α, obtained for systems with 8, 10, and 12 beads and the restitution coefficients $\epsilon=0.92$ and $\epsilon_p=1.0$. The frequencies used are $f=10$, 20, 40, 80, 100, 200, 400, and 800 Hz.

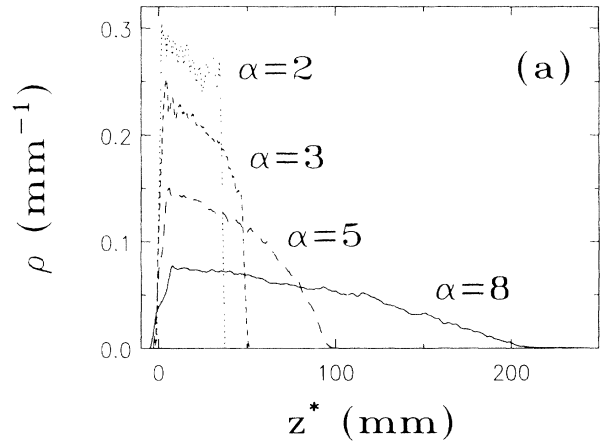

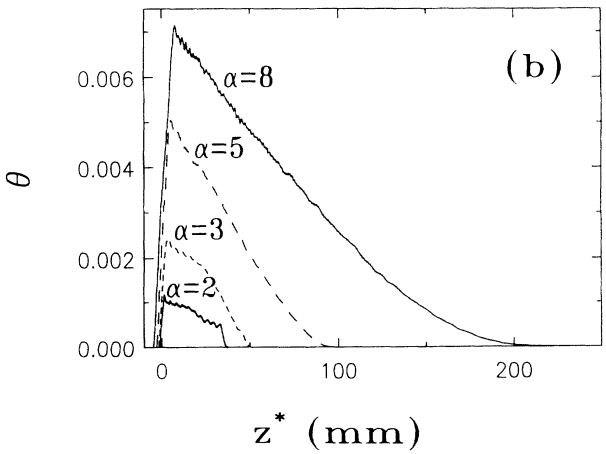

FIG. 5. (a) Shown are the number density profiles $\rho(z^*)$ for $N=10$, $\epsilon=0.92$, $\epsilon_p=1.0$, and $f=20$ Hz as a function of z^* with $d=3$ mm for $\alpha=2$, 3, 5, and 8. (b) Shown are kinetic energy profiles $\theta(z^*)$ for $N=10$, $\epsilon=0.92$, $\epsilon_p=1.0$, and $f=20$ Hz as a function of z^* with $d=3$ mm for $\alpha=2$, 3, 5, and 8.

coordinates $z_i^*(t)$ (introduced in Sec. III) and a diameter of $d=3$ mm. In Fig. 5(a) we show the density profiles $\rho(z^*)$ for different α values (here $\alpha=2$, 3, 5, and 8). We have also evaluated the corresponding kinetic energy profiles, by defining $\theta(z^*)=\langle v(z^*)^2\rangle$. In Fig. 5(b) we plot $\theta(z^*)$ as a function of z^*.

With increasing α the density ρ gets lower and extends to higher z^* (fluidization); furthermore, θ basically decreases with increasing z^*; θ curves belonging to different α values do not cross.

B. The dissipation time in the fluidized regime

The following study is meant to work out the characteristic features of the fluidized regime and the conditions under which *condensation* and/or *clusterization* is obtained. We consider the mean dissipation time τ_D of the energy input at steady state, taking the energy E to be zero when all beads are at rest and lie on the plate. τ_D is the ratio of the average total energy $\langle E\rangle$ of the system at steady state to the input (or equivalently, the output) power $\langle P\rangle$:

$$\tau_D=\frac{\langle E\rangle}{\langle P\rangle}\ . \tag{8}$$

Evidently τ_D measures the energy dissipation in the system: on the time scale of τ_D the kinetic energy which is introduced into the system by the motion of the bottom plate gets dissipated through collisions. We hasten to note that on the average the input power is positive: Although some collisions of the bottom plate may take energy away from the column of beads, on the average the bottom plate feeds energy into the system.

Figure 6 was obtained by following the simulations to times considerably larger than τ_D; displayed is the dissipation time τ_D at steady state, as a function of α. The parameters of the simulation are the same as those used to obtain Fig. 4. We see that all data fall on a master curve which depends on N. Thus $\tau_D f$ is proportional to α and therefore in the fluidized regime

$$\tau_D \propto \frac{2A_0\omega}{g}\ . \tag{9}$$

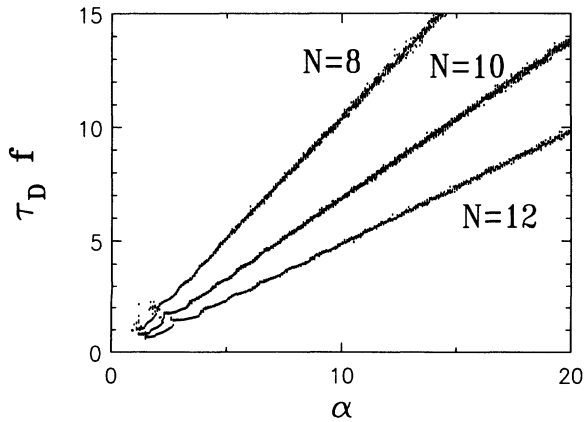

FIG. 6. Shown is the dissipation time τ_D at steady state. The plot gives $\tau_D f$ as a function of α for the same parameters as in Fig. 4.

In Eq. (9) τ_D is proportional to the time of a ballistic flight with initial velocity $A_0\omega$, but for the moment nothing is said about the prefactor, which will be a function of N and ϵ. The dissipation time is larger for smaller N, because this corresponds to a smaller number of dissipative contacts. For small $\tau_D f$ values we observe (as in Fig. 4) a wiggly structure superimposed on the master curves. This is typical for the transition zone between the fluidized and the condensed state.

C. Scaling behavior of the fluidized phase: a crossover acceleration

Now we look for the scaling behavior of the relative height of the center of mass. In the fluidized regime, this quantity is proportional to the total energy and it can be directly measured from the experiments. As we have shown in the preceding subsection, a crossover between a condensed regime and a fluidized regime is evidenced when the dissipation time is of the order of the excitation period. In this subsection we work in the fluidized regime; therefore, for each numerical result, we verified that the dissipation time was much larger than the excitation period. Moreover, we make sure that the simulations have reached a steady state before the average data were produced (i.e., we start the average at $t=10\tau_D$ and end at $t=50\tau_D$).

We denote by $h_{\text{c.m.0}}$ the height of the c.m. when the system rests on the bottom plate; thus $h_{\text{c.m.}}-h_{\text{c.m.0}}$ is diameter independent. Now, from dimensional analysis [and according to Eq. (9)], it is clear that the relative height of the center of mass should scale with a typical velocity square, $(A_0\omega)^2$, the prefactor being a dimensionless function $F(N,\epsilon)$.

$$h_{\text{c.m.}}-h_{\text{c.m.0}}=\frac{A_0^2\omega^2}{g}F(N,\epsilon)\ . \tag{10}$$

To determine the function $F(N,\epsilon)$ we carried out a series of simulations by varying α ($\alpha=10,\ldots,10\,000$), varying N ($N=2,\ldots,100$), and varying ϵ ($\epsilon=0.9995,\ldots,0.01$); ϵ_p is either held equal to one or set to $\epsilon_p=\epsilon$.

In the following we will first find the behavior in the nearly elastic regime. It is clear that the height of the c.m. diverges for $\epsilon\to 1$, since in this case very little energy is dissipated per collision and around this limit fluidization is more likely to occur. Figure 7(a) shows $h_{\text{c.m.}}-h_{\text{c.m.0}}$ as a function of $(1-\epsilon)$ for $\alpha=10$, $\epsilon_p=1$, and $N=5$, 10, and 20. We obtain in the limit $\epsilon\to 1$

$$h_{\text{c.m.}}-h_{\text{c.m.0}}\propto(1-\epsilon)^{-\beta_1}\ , \tag{11}$$

with $\beta_1=1.00\pm0.02$. The next step is to find the N dependence of $h_{\text{c.m.}}-h_{\text{c.m.0}}$. It is obvious that the c.m. is higher for smaller N and vice versa. So we propose that $h_{\text{c.m.}}-h_{\text{c.m.0}}$ should depend on the number of dissipative contacts in the system (which is in our simulations $N-1$ for $\epsilon_p=1$ and N for $\epsilon_p=\epsilon$). Figure 7(b) gives simulation results for $h_{\text{c.m.}}-h_{\text{c.m.0}}$ as a function of $N-1$ for $\alpha=10$, $\epsilon_p=1$, and $\epsilon=0.999$, 0.99, and 0.9. The simulations lead to

$$h_{\text{c.m.}} - h_{\text{c.m.0}} \propto (N-1)^{-\beta_2} , \tag{12}$$

with $\beta_2 = 1.01 \pm 0.02$, i.e., within our accuracy $\beta = \beta_1 = \beta_2 = 1$. Therefore both the N and the ϵ dependence have the same exponent. So we will now introduce the parameter X by setting

$$X = (N-1)(1-\epsilon) \quad \text{for } \epsilon_p = 1 \tag{13a}$$

and

$$X = N(1-\epsilon) \quad \text{for } \epsilon_p = \epsilon . \tag{13b}$$

X seems to be the main variable of the problem as long as it is small. In Fig. 8(a) we plot $h_{\text{c.m.}} - h_{\text{c.m 0}}$ divided by $A_0^2\omega^2/g$ as a function of X found from 4000 realizations of the process using several parameter values. In the fluidized regime all data points fall on the same master curve. Figure 8(a) is plotted in a log-log scale to show clearly the behavior of $h_{\text{c.m.}} - h_{\text{c.m.0}}$; at values $X < 0.1$ the master curve shows a slope around -1. Using the points displayed, we obtain for $F(N,\epsilon)$ introduced in Eq. (10) $F(N,\epsilon) = F(X) = 4/(3X)$, so that the height of the c.m. for small X ($X < 0.1$) can be approximated through

$$h_{\text{c.m.}}^{(0)} = h_{\text{c.m.0}} + \frac{4}{3}\frac{A_0^2\omega^2}{g}\frac{1}{X} . \tag{14}$$

On the other hand, for $X > 0.1$ the data follow a master curve only for $N \gg 1$ and high acceleration. In Fig. 8(b) we fit the data obtained for $\alpha \geq 1000$, $N \geq 20$, and $\epsilon \geq 0.8$ and thus extend the validity of Eq. (14) to the range

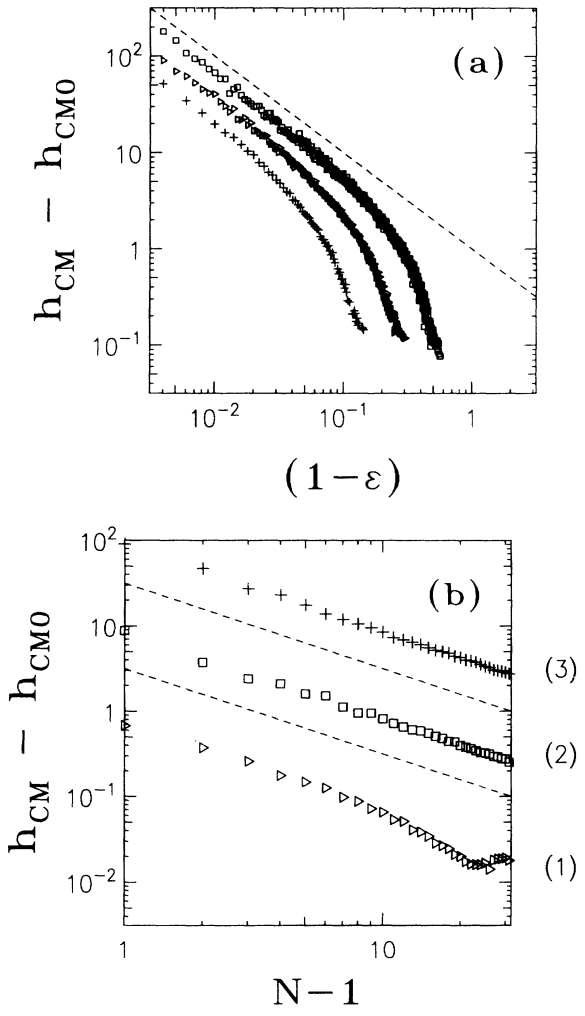

FIG. 7. (a) Plotted is the diameter-independent height of the center of mass as a function of $(1-\epsilon)$ for different N values and for $\alpha = 10$ and $\epsilon_p = 1$. Crosses, triangles, and squares correspond to $N = 20$, 10, and 5, respectively, while the dashed line gives a slope of -1. (b) Plotted is the diameter-independent height of the center of mass as a function of $N-1$, for different ϵ values and for $\alpha = 10$ and $\epsilon_p = 1$. Crosses, squares, and triangles correspond to $1-\epsilon = 10^{-3}$, 10^{-2}, and 10^{-1}, respectively, while the dashed lines give a slope of -1. The notation h_{CM} on the ordinate stands for $h_{\text{c.m.}}$.

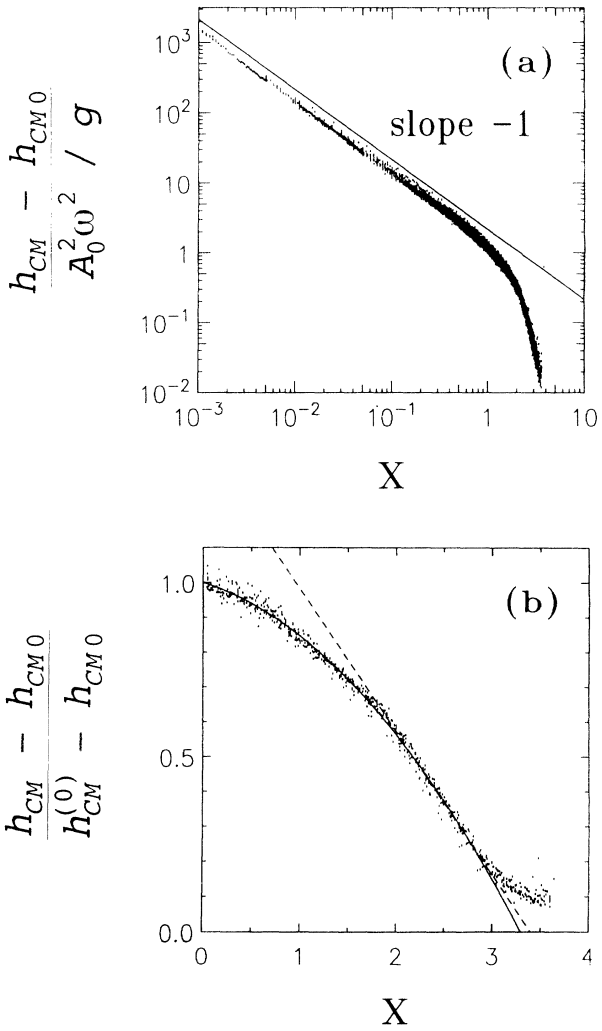

FIG. 8. (a) The height of the center of mass $h_{\text{c.m.}} - h_{\text{c.m.0}}$ as a function of X scaled by $(A_0\omega)^2/g$ for different N values (from 2 to 100), ϵ values (from 0.01 to 0.9995), α values (from 10 to 10000), and $\epsilon_p = \epsilon$ or 1. (b) The height of the center of mass $h_{\text{c.m.}} - h_{\text{c.m.0}}$ as a function of X scales by $h_{\text{c.m.}}^{(0)} - h_{\text{c.m.0}}$ for different N values (from 20 to 100), ϵ values (from 0.2 to 0.9995), large α values ($\alpha = 10000$), and $\epsilon_p = \epsilon$ or 1. The dashed line gives a first-order polynomial fit with root $X = 3.17$, the full line gives a second-order polynomial fit with root $X = 3.09$.

$X \leq 2.8$, by setting

$$h_{\text{c.m.}}^{(1)} = h_{\text{c.m.}0} + \frac{4}{3}\frac{A_0^2\omega^2}{g}\frac{\varphi(X)}{X} , \tag{15a}$$

with

$$\varphi(X) = 1 - a_1 X - a_2 X^2 , \tag{15b}$$

where the constants are $a_1 = 0.098$ and $a_2 = 0.073$.

This expression was obtained through a polynomial fit in the interval from 0 to 2.8. As can be seen from Fig. 8(b), for $X > 2.8$ the displayed curve changes from being concave to being convex. Equations (15a) and (15b) extrapolate to an intersection with the real axis at $X = X_c = 3.09$. A linear data fit [plotted as a dashed line in Fig. 8(b) and carried out in the interval from 2 to 2.8] leads to an intersection at $X = X_c = 3.17$. These findings suggest that (in the absence of additional effects) clusterization occurs around $X_c \cong 3.1$. Indeed for $X > X_c$ one never reaches a fluidized phase, regardless of the acceleration. On the other hand, in the intermediate region (i.e., for $2.5 < X < 4$) and for very large accelerations (α values between 10^4 and 10^6) the simulations lead to the separation of the column into an array of beads condensed at the bottom and of several beads fluidized at the top. Thus for X above X_c the dissipation inside the column is so important that no complete fluidization ever occurs and the lower part of the column stays condensed. This means here that the motion of the lower beads is always correlated. We can relate our X_c value to the work of Bernu and Mazighi [8], who find $X_c' = \pi$ (see Appendix B) for a column of balls colliding with a wall. Note, however, that the situation investigated by Bernu and Mazighi is different from ours: They monitor the dissipation of the *initial* internal energy; we have a steady influx of energy into the system. This difference may also be the reason why we obtain for $X > X_c'$ partially condensed states.

In a way similar to the above we establish the scaling behavior of the dissipation time τ_D, obtaining

$$\tau_D = \pi\frac{A_0\omega}{g}\frac{\varphi'(X)}{X^\gamma} , \tag{16a}$$

where

$$\varphi'(X) = 1 - a_3 X - a_4 X^2 . \tag{16b}$$

Again the data were fitted in the interval from 0 to 2.8; the values of the parameters are now $a_3 = 0.087$, $a_4 = 0.065$, and $\gamma = 1.5$.

From Eq. (16) we infer now a condition for fluidization in the range $X < X_c$. In the fluidized regime the time scale of energy dissipation is much larger than one period. Thus we use $\tau_D f \gg 1$ as a criterion for fluidization. Translated in terms of the acceleration α this gives

$$\alpha \gg \alpha_c \equiv 2\frac{X^\gamma}{\varphi'(X)} . \tag{17}$$

This result is well corroborated by further simulations.

V. EXPERIMENTAL RESULTS

A. The case of high restitution coefficients: steel beads

The following experiments were performed using steel beads. First we measured the value of the restitution coefficient, by determining the height of rebound for a bead dropped from a height of 1 m on a smooth block of the same material. In this way we found $\epsilon = 0.90 \pm 0.05$.

With the help of a video camera connected to an image processing device, we accumulated images of the light dots formed at the center of the beads by a remote light source. The results allow us to access experimentally the density profile of the column of beads. From such profiles we extract the height of the center of mass $h_{\text{c.m.}}$ (here a diameter-dependent quantity). We compare these data to the corresponding computer simulations; the best fits to all our experimental data are obtained for $\epsilon = 0.92 \pm 0.01$, while we take $\epsilon_p = 1$. The data obtained in three experimental runs with steel beads are presented in Figs. 9(a)–9(e); the curves show $h_{\text{c.m.}}$ as a function of α and N. The first set of data is displayed in Figs. 9(a) and 9(b) where the frequency was set at $f = 16.5$ and 15 Hz, while the amplitude A_0 was varied. The second set of experiments was performed at amplitudes $A_0 = 3.42$ and 1.96 mm, while the frequency was varied [see Figs. 9(c) and 9(d)]. In the third set of experiments we kept the amplitude $A_0 = 2.98$ mm and the frequency $f = 15$ Hz constant and we varied the number of beads N; the results are shown in Fig. 9(e). In all these figures we plot the simulation results as small squares, the experimental data as circles, and the limiting scaling laws for the fluidized regime as continuous curves [see Eq. (15)]. We are now in the intermediate α regime, in which the simulations exhibit a complicated resonant behavior as discussed in Sec. IV. The scaling predictions of the fluidized phase agree well with the experimental results, although not all theoretical details are reproduced: Thus the wiggly structure does not appear, possibly due to disturbances induced by the friction with the walls, a fact which may destabilize the organization of the column and therefore cause a disordered regime to occur more rapidly.

In Fig. 10 we compare the experimental density profile (here $N = 10$, $A_0 = 2$ mm, and $f = 21$ Hz) with the simulation results in the fluidized regime for $\epsilon = 0.92$; overall we find that the agreement is fair. Hence the experimental data can indeed be understood from simulations, in which a single parameter (namely $\epsilon = 0.92$) enters.

B. The case of low restitution coefficients: aluminum beads

Here we report our experimental findings with aluminum beads. Experimentally we measured the restitution coefficient for aluminum beads to be $\epsilon = 0.60 \pm 0.05$. Again the column consists of $N = 10$ beads. The behavior of the column of beads is now vastly different from what we found previously; in fact the column behaves as a condensed block. We found it convenient to measure the time between two collisions of this block with the bottom plate; we denote this time by T_{coll}. The time T_{coll} is determined as a function of the normalized

acceleration α, by recording the sound created by the heap when colliding with the bottom plate. In Fig. 11 we plot on the same diagram the experimental findings and the results of two numerical simulations for $N=10$, $\epsilon=\epsilon_p=0.6$ and for $N=1$, $\epsilon_p=0$. The simulation results for these two cases practically coincide in the range displayed in the figure, and hence lead only to one curve (denoted by triangles).

We recall now that in the one-bead problem a series of bifurcations occurs [18,19], which involve a set of fundamental modes that are multiples of the lowest fundamental period $T=1/f$. Our experimental findings with aluminum beads, given in Fig. 11, parallel this picture in that the experiments display clearly the first two bifurca-

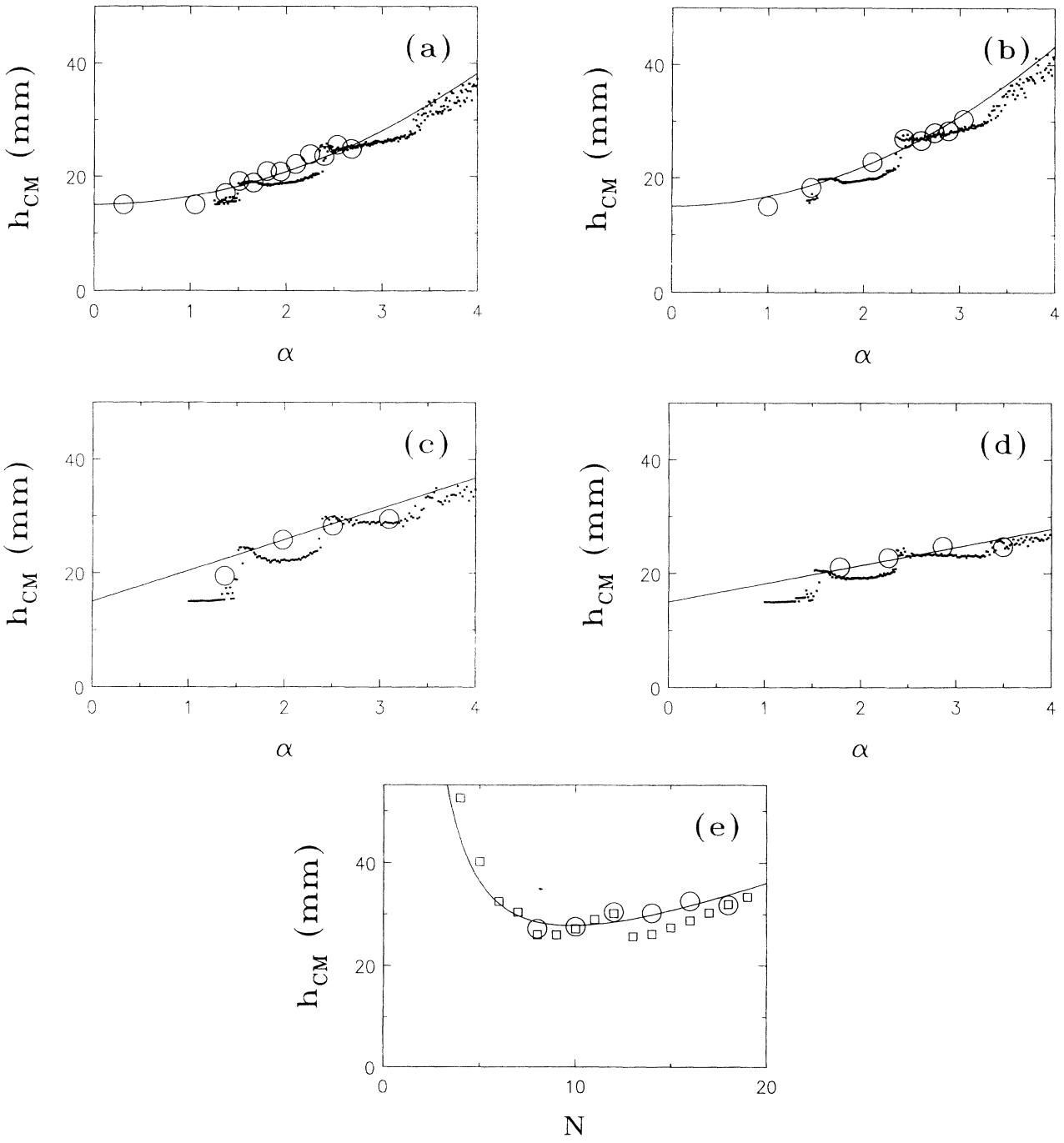

FIG. 9. (a) Experimental (circles), simulation (dots), and fit (full line) results for the height of the center of mass $h_{c.m.}$ of $N=10$ beads (here diameter dependent with $d=3$ mm) as a function of α. The frequency is $f=16.5$ Hz and the restitution coefficients are $\epsilon=0.92$ and $\epsilon_p=1$. (b) The same results as in (a) but the frequency is here $f=15$ Hz. (c) The same results as in (a) but here we varied the frequency and held the amplitude constant, $A_0=3.42$ mm. (d) The same results as in (c) but the amplitude here is $A_0=1.97$ mm. (e) The same results as in (a) with $A_0=2.98$ mm, $f=15$ Hz, and $N=8$, 10, 12, 14, 16, and 18. The simulations here are depicted by squares.

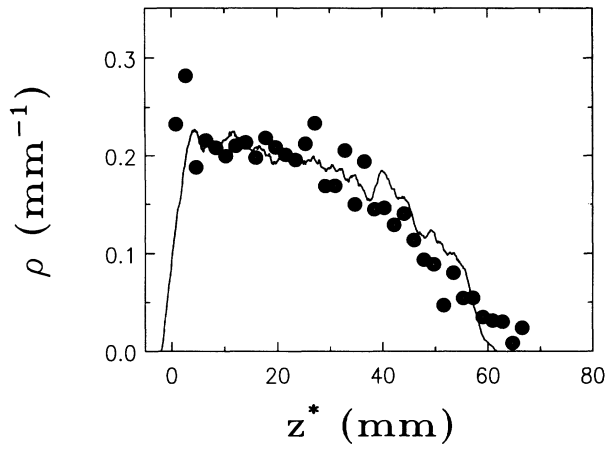

FIG. 10. The number density ρ as a function of the height z^*; compared are experiment (circles) and simulation (line) for $N=10$, $f=21$ Hz, $A_0=1.97$ mm, $\epsilon=0.92$, and $\epsilon_p=1$.

tions, whose onset mirrors nicely the simulation results. How far the bifurcation cascade can be monitored is an interesting question since even in a dissipative one-ball system fully developed chaos should not show up [34].

VI. DISCUSSION AND CONCLUSIONS

In this article we studied a one-dimensional column of beads undergoing vertical vibrations. We presented experiments and numerical simulations using an event-driven algorithm, suited to deal both with the fluidized and with the extremely condensed phase. Thus we have achieved a direct dynamical assessment of a numerical model on a tailored granular system. As stressed, in this system a progressive transition takes place between a *condensed* phase, where the dilatation is close to zero and the beads' motion is collective, to a *fluidized* phase, where the beads' motion is erratic. We found that the position of the transition regime is controlled by the relative acceleration of the plate. At low accelerations the Fourier spectrum of the c.m. motion shows subharmonic

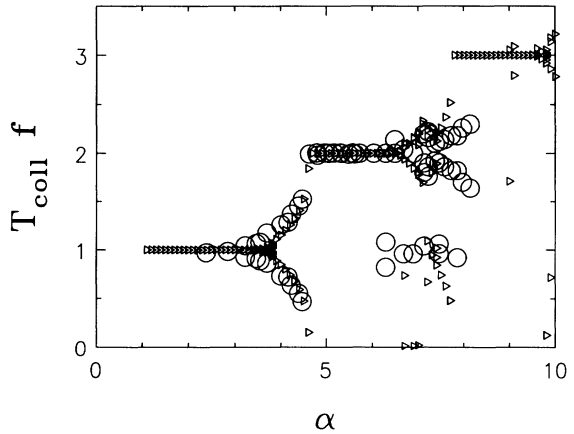

FIG. 11. Times between collisions, $T_{\rm coll}$, with the bottom plate in experiments (circles) and simulations (triangles) for $N=10$ and $f=30$ Hz. Plotted is $T_{\rm coll}f$ versus α. The simulations use $\epsilon=\epsilon_p=0.6$.

responses, which reproduce a Feigenbaum-type scenario, interrupted by series of fluidized and chaotic regimes. In this case, the column behaves for all practical purposes as a condensed block, with long phases of motion where all beads have almost the same velocity but are not necessarily in contact. An important point is that the acceleration which determines the onset of the transition regime may get to be extremely large in the case of low restitution coefficients and/or high number of beads. For one inelastic bead this highly dissipative behavior was studied by Mehta and Luck [20], who evidenced the appearance of a complex pattern of bifurcations.

Furthermore we evaluated, as a function of the parameters ϵ and N, the acceleration, Eq. (17), needed to reach the fluidized phase for all the beads. When $N\gg1$ we showed that the acceleration scales with $X=N(1-\epsilon)$. In particular, for very high accelerations α and for $X>X_c$ (say $X_c\cong3.1$) we never found that the whole column fluidizes. Instead, for $2.5<X<4$ we find that the column separates into an array of condensed beads at the bottom and into several fluidized beads at the top. For very low accelerations we observe that the column moves as a block, so that no fluidization occurs. For $X<X_c$ we found that these clusters may separate due to a collision with the bottom plate, while for $X>X_c$ a clustered block stays clustered. Furthermore, we related the threshold value X_c to the findings of Bernu and Mazighi in the study of a column of beads hitting a wall (there no gravity was involved); in our case we found a variety of additional effects, since here energy is steadily fed into the system.

The agreement between experiments and numerical simulations is good. We observe both the predicted fluidized behavior at high restitution coefficients (here steel beads) and condensation as well as clusterization for low restitution coefficients (aluminum beads). For small X we are able to show that the density profiles scale; for large X ($X=4$) we observe a bifurcation scenario. Nevertheless, not all details of the complex resonant behavior predicted by the simulations could be found experimentally.

It is worth noticing that some of the features of the response of a vibrated 1D column reappear, at least qualitatively, also in higher dimensions. In 2D and 3D bifurcation scenarios are observed [2,3,20]. Fluidization is also evidenced in 2D and 3D; there it coexists with the condensed phase (in fact one has surface fluidization). Similarly to the 1D case, surface fluidization was shown to be strongly dependent on the internal dissipation of the granular material [2].

ACKNOWLEDGMENTS

LAOMC is an U.R.A. of the CNRS and this work was supported by a special grant A.T.P. "Matière en grain." We thank J. Lanusa for efficient technical assistance and Professor M. Jean, Professor B. Bernu, and Professor R. Mazighi for interesting discussions. The support of the Deutsche Forschungsgemeinschaft (SFB 60), of the Fonds der Chemischen Industrie, and of the PROCOPE scientific collaboration program is acknowledged.

APPENDIX A

Using the event-driven algorithm presented in Sec. III we are able to simulate the fluidized regime very effectively. This is so because the computing time is proportional to the number of events, and not (as in molecular-dynamics simulations) to the number of time steps. In the fluidized regime the times between collisions are large and beads move independently of each other. In the condensed regime the time intervals between collisions decrease (e.g., Fig. 2) and several beads get close and move in a correlated way [compare Figs. 3(b) and 3(c)]. In the following we describe an alternative algorithm which is able to get rid of collisions occurring at extremely short time intervals. This algorithm is similar in spirit to the procedure for individual beads but is also able to handle clusters.

1. The handling of clusters in an event-driven procedure

Formally, we introduce the concept of clusters as systems of beads in contact. We let two objects turn into a cluster if their relative velocities after an event lie below a certain value v_c; then we set their relative velocities to zero. As long as there is no cluster in the system, the normal event-driven procedure increases time with time steps Δt_i defined in Eq. (3). These time steps get to be very small for objects almost in contact (see Fig. 2). Then many processes happen almost simultaneously. To speed up the algorithm we developed the largest-relative-velocity (LRV) procedure. For this we compute all relative velocities $\Delta v_i = v_{i-1} - v_i$ between all pairs $(i, i-1)$ of clustered objects. Objects with $\Delta v_i \leq 0$ do not collide, whereas the objects with $\Delta v_i > 0$ are bound to interact.

The LRV procedure works as follows: we pick out the maximal value of the set (Δv_i), say $\Delta v_j = \max(\Delta v_i)$, and let the corresponding pair (say $j, j-1$) collide. The velocity changes are computed, using the same collision matrices as defined in Eqs. (4) and (5); then the set (Δv_i) of relative velocities gets updated. The above procedure is repeated until all Δv_i of objects in a cluster are less than or equal to v_c (some Δv_i can become, of course, negative, in which case some beads leave the cluster).

Now we will discuss the special cases which involve collisions of clusters. On the first view we may differentiate whether the bottom plate is involved in the collision or not; this leads to three possible situations to be accounted for. If the bottom plate is not involved collisions occur between two clusters, say with N_1 and N_2 beads each. If the bottom plate is involved we have a cluster (N_1) colliding with the bottom plate, or a cluster (N_1) that collides with another cluster (N_2) which rests on the bottom plate. These situations include as special cases the simple binary collisions of one bead with the bottom plate or with another bead (one bead is a special case for a cluster). These three distinct situations are handled on the same footing by the LRV procedure; they differ, however, physically, due to the very large mass (assumed infinite) of the bottom plate. We consider them one by one.

(1) Collisions of two clusters. In a collision involving two clusters of sizes N_1 and N_2, a total number of $M = N_1 + N_2$ objects are in contact which means in 1D a total of $M-1$ interacting pairs. To visualize this case we plot in Fig. 12 the trajectories of two columns of $N_1 = 2$ and $N_2 = 3$ beads each during a collision; the computation was performed with the restitution coefficient $\epsilon = 0.8$.

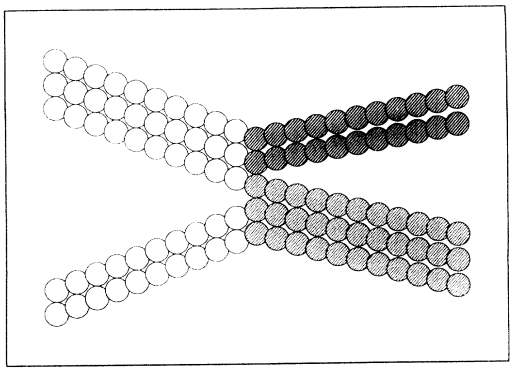

FIG. 12. Trajectories of five beads, initially in two clusters, for $\epsilon = 0.8$.

To test the outcome of the LRV procedure we look at what happens when the initial separation s between the beads decreases towards zero. Thus we carry out a series of simulations in which we vary s; we take it to be $s = 10^{-3}, 10^{-4}, 10^{-5}, 10^{-6}$, and 0 m. The simulations for $s > 0$ are performed in the event-driven fashion, whereas for $s = 0$ LRV is used. In all simulations the center of mass is a conserved quantity; for identical initial conditions (except s) the trajectories after the collisions coincide quantitatively for all $s \leq 10^{-5}$ m. Thus the LRV procedure reproduces the behavior of two colliding columns of beads very well when s is small.

(2) Collisions of one cluster with the bottom plate. To illustrate this case we plot in Fig. 13 a cluster of beads $(N_1 = 5)$ that hits the bottom plate; here we take $\epsilon = 0.9$ and $\epsilon_p = 1.0$. This special case computed in the LRV formalism can be directly compared to the results of the independent-collision wave (ICW) model introduced by Bernu and Mazighi [8]. The ICW formalism uses for one

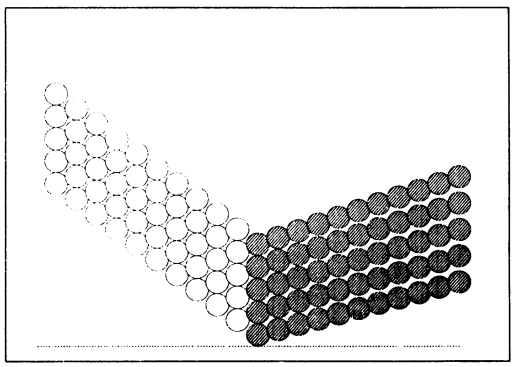

FIG. 13. Trajectories of five beads, initially in one cluster, which hits the bottom plate. The restitution coefficients are $\epsilon = 0.9$ and $\epsilon_p = 1$.

collision wave the transfer matrix **Y** such that $u_i = Y_{ij} v_j$, where u_i and v_j are the velocities of the particles before and after the collisions, respectively. **Y** is an ordered product of $(N+1)(N+1)$ matrices; say for one collision wave from below

$$Y_n = D_{n-1,n} D_{n-2,n-1} \cdots D_{1,2} D_{0,1} \ . \tag{A1}$$

The $D_{i-1,i}$ are related to the $C_{i-1,i}$ of Eqs. (4) and (5); they have an almost diagonal form:

$$D_{i-1,i} = \begin{bmatrix} 1 & & & & & & \\ & \ddots & & & 0 & & \\ & & 1 & & & & \\ & & & C_{i-1,i} & & & \text{row } i-1 \\ & & & & 1 & & \text{row } i \\ & 0 & & & & \ddots & \\ & & & & & & 1 \end{bmatrix} . \tag{A2}$$

For small X [see Eq. (13)] (say $\epsilon = 0.9$ and $N = 5$) the collision waves do not interfere and we find that the ICW and the LRV models lead to exactly the same results. The difference in the velocity of the beads is smaller than 10^{-12} m/s after the collision. At these low X values the order of collisions is indistinguishable in the two models. For large X (say $\epsilon = 0.6$ and $N = 5$) the order of collisions in the two models does not coincide anymore, since different collision waves catch up with each other and interfere.

(3) Collisions of a cluster resting on the plate with another cluster. As in Figs. 12 and 13 we carry out the sequence of collisions in the order specified by the LRV procedure when the clusters hit each other. As an example for this case we plot in Fig. 14 the situation when $N_1 = 3$ beads hit $N_2 = 2$ beads which rest on the bottom plate.

2. A test for the cutoff velocity

When the relative velocity of two objects drops below the cutoff velocity v_c we merge in the LRV procedure these objects into a cluster. This leads to a transition from a condensed (but still separated) stack of objects to a cluster of objects in contact. In the stack the times between collisions do not vanish in general, whereas in the cluster the times between collisions are zero. Thus we have to choose the arbitrary cutoff velocity v_c to be orders of magnitude lower than the typical velocity of the system, given, say, by $A_0\omega$. In an independent series of simulations we have tested the dependence of the height of the center of mass $h_{\text{c.m.}}$, of the dissipation time τ_D, and of the mean dilatation λ on the value of v_c. We find that the choice of v_c does not influence these quantities, as long as $v_c \ll A_0\omega$. In Fig. 15 we display the height of the center of mass $h_{\text{c.m.}}$ (triangles), the dissipation time τ_D (circles), and the mean dilatation λ (squares) versus v_c of a system of $N = 10$ beads with $A_0\omega = 0.25$ m/s, $\epsilon = 0.9$, and $\epsilon_p = 1$. These values do not change as long as we choose v_c such that $v_c < 10^{-4}$ m/s; thus when computing $h_{\text{c.m.}}$, τ_D, or λ taking v_c below 10^{-4} m/s allows us to decrease the computing time without affecting the outcome of the simulations.

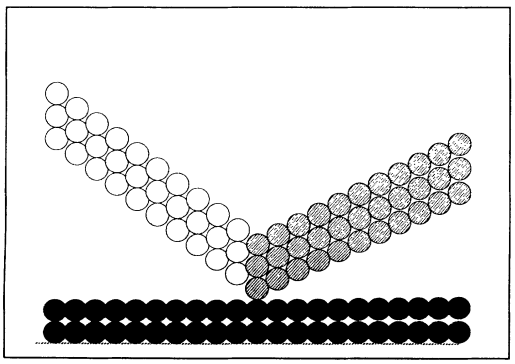

FIG. 14. Trajectories of three beads in a cluster which hits a cluster of two beads resting on the bottom plate. The restitution coefficients are $\epsilon = 0.9$ and $\epsilon_p = 1$.

APPENDIX B

In a recent article Bernu and Mazighi [8] investigated the problem of a column of N beads hitting a wall which moves with a constant velocity (in Ref. [8] no gravity was involved). One of the findings of Ref. [8] was that below a critical value of the restitution coefficient ϵ_c the beads condense on the wall. Now ϵ_c was found to be independent of the initial state of agitation of the beads, but to be a function of the number N of beads [8]:

$$\epsilon_c = \tan^2\left[\frac{\pi}{4}\left[1-\frac{1}{N}\right]\right] . \tag{B1}$$

In the limit $N \gg 1$ this leads to $\epsilon_c \cong 1 - \pi/N$ or to

$$X_c' = \pi \ , \tag{B2}$$

where $X_c' = N(1-\epsilon_c)$ is the value above which clusteriza-

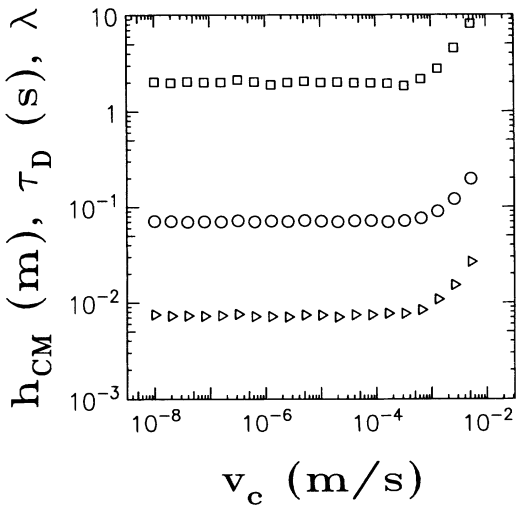

FIG. 15. Results for $h_{\text{c.m.}}$ (triangles), τ_D (circles), and λ (squares) obtained as a function of the cutoff velocity v_c. Here $N = 10$, $A_0\omega = 0.25$ m/s, $\epsilon = 0.9$, and $\epsilon_p = 1$. Below 10^{-4} m/s, the data are independent of v_c.

tion of the column of beads occurs. Physically it corresponds to the possibility for a column of beads to cluster on a moving plate independently of the initial velocities in the column. From our simulations we found that in the fluidized phase the relevant parameters (i.e., height of the center of mass and dissipation time) scale with $X=N(1-\epsilon)$ for $N \gg 1$. The behavior of, for example, the height of the c.m. can be fitted with a parabola in the interval from 0 to 2.8, see Eq. (15). This fit leads to an extrapolated value $X_c \cong 3.1$ for the intercept with the x axis. Since our simulations are dynamic and energy is steadily fed into the system we cannot expect $h_{\text{c.m.}}$ to vanish. Indeed, for $X > 2.8$ we find deviations from the simple pattern, a fact which indicates a more complex behavior of the column.

[1] H. M. Jaeger and S. R. Nagel, Science **255**, 1523 (1992).
[2] E. Clément and J. Rajchenbach, Europhys. Lett. **16**, 149 (1991).
[3] E. Clément, J. Duran, and J. Rajchenbach, Phys. Rev. Lett. **69**, 1189 (1992).
[4] P. A. Thompson and G. S. Grest, Phys. Rev. Lett. **67**, 1751 (1990).
[5] P. A. Cundall and O. D. L. Strack, Geotechnique **29**, 47 (1979).
[6] J. J. Moreau, in *Nonsmooth Mechanics and Applications*, edited by J. J. Moreau and P. D. Panagiotopoulos (Springer-Verlag, New York, 1988), pp. 1–82.
[7] B. D. Lubachevsky, J. Comput. Phys. **94**, 255 (1991).
[8] B. Bernu and R. Mazighi, J. Phys. A **23**, 5745 (1990).
[9] S. McNamara and W. R. Young, Phys. Fluids A **4**, 496 (1992).
[10] S. McNamara and W. R. Young, Phys. Fluids A **5**, 34 (1993).
[11] M. P. Allen and D. J. Tildesley, *Computer Simulation of Liquids* (Oxford University Press, Oxford, 1987).
[12] E. Clément, S. Luding, A. Blumen, J. Rajchenbach, and J. Duran, Int. J. Mod. Phys. B **7**, 1807 (1993).
[13] S. F. Foerster, M. Y. Louge, H. Chang, and K. Allia (unpublished).
[14] S. B. Savage, J. Fluid Mech. **92**, 53 (1979).
[15] S. B. Savage, in *Disorder and Granular Media*, edited by D. Bideau (North-Holland, Amsterdam, 1993).
[16] P. Evesque and J. Rajchenbach, Phys. Rev. Lett. **61**, 44 (1989).
[17] S. Douady, S. Fauve, and C. Laroche, Europhys. Lett. **8**, 621 (1989).
[18] S. Celashi and R. L. Zimmermann, Phys. Lett. A **120**, 447 (1987).
[19] P. Pieranski, J. Phys. (Paris) **44**, 573 (1983).
[20] A. Mehta and J. M. Luck, Phys. Rev. Lett. **65**, 393 (1990).
[21] J. A. C. Gallas, H. J. Herrmann, and S. Sokolowski, Phys. Rev. Lett. **69**, 1371 (1992).
[22] J. A. C. Gallas, H. J. Herrmann, and S. Sokolowski, Physica A **189**, 437 (1992).
[23] Yi Zhang and C. S. Campbell, J. Fluid Mech. **237**, 541 (1992).
[24] T. A. J. Duke, G. C. Barker, and A. Mehta, Europhys. Lett. **13**, 19 (1990).
[25] D. C. Hong and J. A. McLennan, Physica A **187**, 159 (1992).
[26] P. C. Johnson and R. Jackson, J. Fluid. Mech. **176**, 67 (1987).
[27] Y.-H. Taguchi, Phys. Rev. Lett. **69**, 1367 (1992).
[28] R. Mazighi, B. Bernu, and F. Deylon (unpublished).
[29] M. Jean and J. J. Moreau (unpublished).
[30] Additional works by J. J. Moreau and M. Jean as well as by B. Bernu and R. Mazighi on similar models are in progress (private communication).
[31] H. J. Hermann, J. Phys. (Paris) II **3**, 427 (1993).
[32] S. F. Edwards and R. B. S. Oakeshott, Physica A **157**, 1080 (1989).
[33] C. K. K. Lun, S. B. Savage, D. J. Jeffrey, and N. Chepurny, J. Fluid. Mech. **140**, 223 (1983).
[34] J. M. Luck and A. Mehta, Phys. Rev. E **48**, 3988 (1993).

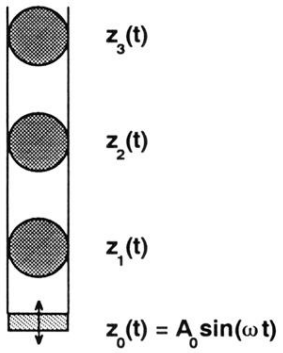

FIG. 1. Model system with a vibrating bottom plate; here three beads are shown.

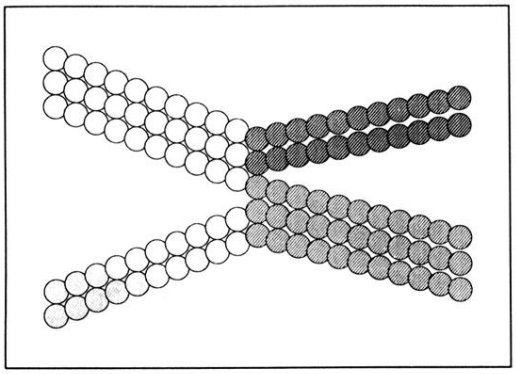

FIG. 12. Trajectories of five beads, initially in two clusters, for $\epsilon=0.8$.

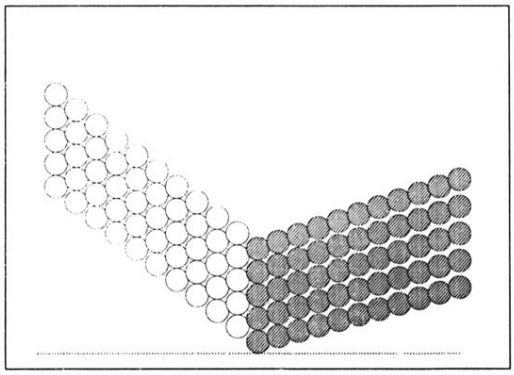

FIG. 13. Trajectories of five beads, initially in one cluster, which hits the bottom plate. The restitution coefficients are $\epsilon=0.9$ and $\epsilon_p=1$.

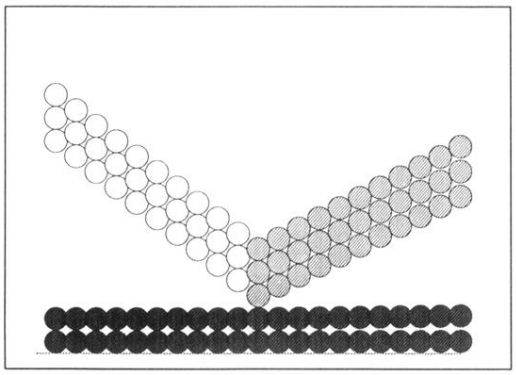

FIG. 14. Trajectories of three beads in a cluster which hits a cluster of two beads resting on the bottom plate. The restitution coefficients are $\epsilon=0.9$ and $\epsilon_p=1$.

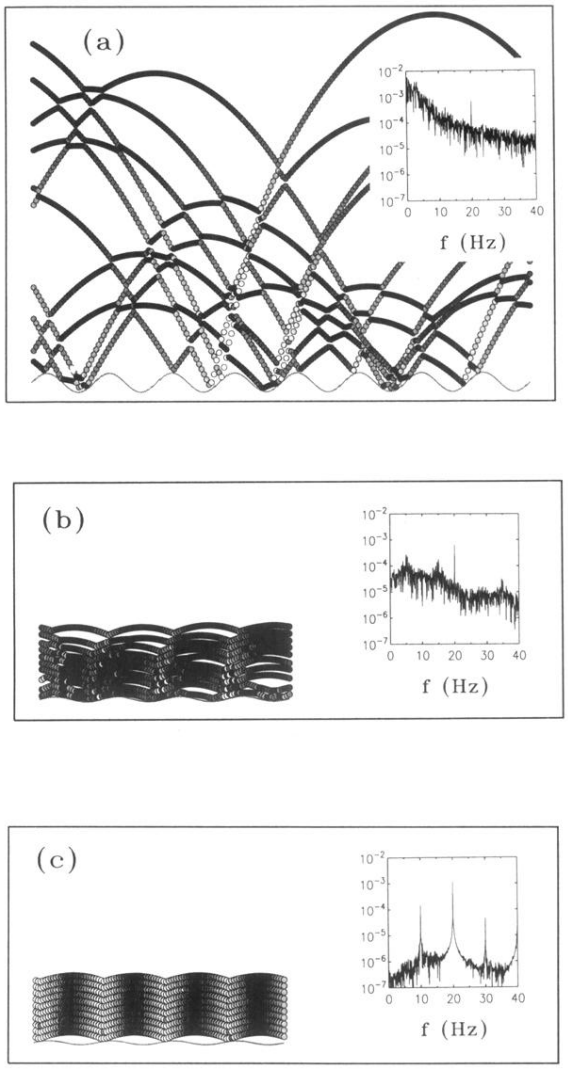

FIG. 3. (a) Motion of ten beads for $f=20$ Hz, $\alpha=8.0$, $\epsilon=0.92$, and $\epsilon_p=1$. The inset displays the frequency spectrum for the motion of the center of mass (c.m.). (b) Motion of ten beads for $f=20$ Hz, $\alpha=2.0$, $\epsilon=0.92$, and $\epsilon_p=1$. The inset displays the frequency spectrum for the motion of the center of mass. (c) Motion of ten beads for $f=20$ Hz, $\alpha=1.5$, $\epsilon=0.92$, and $\epsilon_p=1$. The inset displays the frequency spectrum for the motion of the center of mass.